2-D Van Atta Array of Wideband, Wideangle Slots for Radiative Wireless Power Transfer Systems

M. Ettorre, W.A. Alomar, A. Grbic

2D Van Atta Array of Wideband, Wideangle Slots for Radiative Wireless Power Transfer Systems

Mauro Ettorre, *Senior Member, IEEE*, Waleed A. Alomar, and Anthony Grbic, *Fellow, IEEE*

***Abstract*—We present a two-dimensional Van Atta array for far-field wireless power transfer systems. The antenna array is made up of wideband, wideangle long slots. The monostatic radar cross section (RCS) of the finite array is derived by windowing the aperture field distribution of the corresponding infinite case. It is shown that for over-sampled apertures, the array behaves as an ideal Van Atta reflector. Therefore, the proposed solution can collect and reradiate the total power impinging on it from a remote source over a large field of view and bandwidth. The array design is presented and validated through measurements over a relative bandwidth of 24% centered at a frequency of 5.8 GHz. The array consists of four slots, each fed by eight coaxial ports. Coaxial cables are used to connect pairs of feeds in a Van Atta configuration. A bi-directional amplifier is also introduced into the Van Atta scheme to amplify the collected energy before re-transmission to a possible moving user for wireless power transfer. Off-the-shelf components are used to implement the bi-direction amplifier. The amplifier is matched across the bandwidth of the array and provides 5 dB gain. Monostatic RCS measurements show that the array exhibits -10dB beamwidths of about 118° and 80° in the E- and H-planes, over the entire bandwidth. In addition, it is shown that when the array ports are terminated with matched loads, the antenna RCS is reduced by approximately -15 dB with respect to the Van Atta case. This experimentally confirms that the array collects the total energy impinging from a remote source.**

***Index Terms*—Van Atta antennas, time reversal, retrodirective antennas, wideband arrays, wireless power transfer.**

I. Introduction

WIRELESS power transmission (WPT) will change our daily experience with electronic devices in the years to come. One can envision electronic devices in need of energy being tracked and recharged by a power unit in close proximity [1], [2]. For example, a rechargeable electronic device in need of energy may emit a beacon signal that is received by a power unit in the area. The power unit can then track the electronic device and send back an amplified signal for power recharging [3]–[5]. In such a scenario, the antennas of the power unit and the electronic device are assumed in their respective far field. For this reason, these systems are named far-field WPT systems as a difference with those using inductive near-field coupling for wireless power transmission [1], [2].

Far-field WPT systems present several challenges for the antenna in the power unit. The antenna should be able to detect and track a moving user over a large angular range in a room or public environment [3], [5]. At the same time, the antenna should be able to direct the energy toward the electronic device to avoid unwanted electromagnetic interactions and minimize the exposure of human beings to electromagnetic radiation [5]. Antenna systems capable of automatically tracking the direction of arrival of an unknown incoming signal are known as retrodirective antennas [6]-[9]. They typically consist of arrays of simple radiating elements (generally dipoles, patches, etc.) connected to a circuit network that phase conjugates the impinging field in order to reradiate it in the incoming direction. Retrodirective antennas have been largely deployed in applications such as mobile and satellite communication systems, radars [8], [9] and microwave power transmission [10].

Phase conjugation of the field impinging on the retrodirective antenna is generally realized using a Van Atta approach [11] or more advanced heterodyne or digital schemes [8], [9], [12], [13]. In the Van Atta case, the antenna elements of a regularly spaced array are connected in pairs with equal length transmission lines. The connections allow the phase profile of the imping signal to be reversed without resorting to active circuitry. In a recent paper [14], the authors have shown that for far-field WPT Van Atta antennas provide the same focusing capabilities as more sophisticated approaches but with a reduced cost and simpler implementation. In addition, the scanning and bandwidth capabilities of Van Atta solutions are only limited by the antenna employed [9].

Van Atta antennas are generally based on arrays of resonant radiating elements such as dipoles or patches [3], [4]. These arrays have a narrow bandwidth and limited field of view, as shown in several papers [3], [4], [15]-[18]. In addition, they backscatter more than 50% of the incoming energy [14]. In [14], we proposed an array of long slots to overcome these limitations. The monostatic RCS of a Van Atta array of long slots is derived here by windowing the aperture field distribution of the corresponding infinite array [21]. It is shown that, for over-sampled apertures, the array behaves as an ideal Van Atta reflector. The complete design of an array consisting of four slots is then presented and validated experimentally. Each slot of the array is fed by eight coaxial

This work was supported by the King Abdulaziz City for Science and Technology (KACST) - University of Michigan Center for Microwave Sensor Technology. M. Ettorre would like to thank CNRS and the University of Rennes 1, Rennes, France for their support and financial contribution.

M. Ettorre is with the Institute of Electronics and Telecommunications of Rennes (IETR), UMR CNRS 6164, University of Rennes 1, 35042 Rennes, France. A the time of this work he was on a sabbatical in the Radiation Laboratory, Department of Electrical Engineering and Computer Science, University of Michigan, Ann Arbor, MI 48109-2122 USA. e-mail: mauro.ettorre@univ-rennes1.fr).

W. A. Alomar is with the Communication and Information Technology Research Institute (CITRI), KACST, Saudi Arabia.

A. Grbic is with the Radiation Laboratory, Department of Electrical Engineering and Computer Science, and the Center of Photonic and Multiscale Materials (C-PHOM), University of Michigan, Ann Arbor, MI 48109-2122, USA. e-mail: agrbic@umich.edu.

ports (input ports). The antenna is made of aluminum and fabricated using a standard CNC milling process. Simulation results show a relative bandwidth of 24% over a $\pm 40^\circ$ field of view in elevation along the principal planes of the antenna. Van Atta operation is achieved by connecting pairs of input ports with coaxial cables of equal length. Monostatic RCS measurements show that the antenna can redirect an incoming signal over a large relative bandwidth (24%) and field of view in both its E- (118°) and H-plane (80°). Further, it is shown that when the input ports are terminated with matched loads, the antenna absorbs the total incoming power. Finally, a bi-directional amplifier made from off-the-shelf components is used to enhance the RCS of the Van Atta array. Measurements show that the RCS is augmented by more than 10 dB with the respect to the case when the amplifiers are powered off.

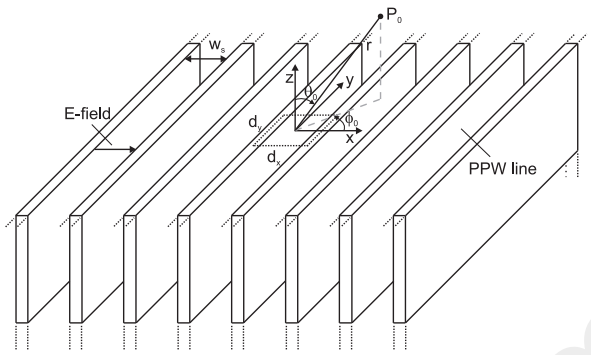

Fig. 1. The geometry of the array of long slots. The slots at $z = 0$, with width w_s, are fed by air-filled parallel plate waveguide (PPW) lines. The observation point P_0 is denoted by its spherical coordinates (r, θ_0, ϕ_0); d_x and d_y are the periods along the x- and y-axis, respectively.

The paper is organized as follows. Section II derives the monostatic RCS of a finite Van Atta array of long slots. Section III presents the design of the proposed array of long slots. Full-wave simulation results of the bandwidth and scanning capabilities of the antenna along its principal scanning planes are reported. The fabrication process and antenna prototype are discussed in Section IV. Section IV also introduces the bi-directional amplifier. Section V presents the monostatic RCS measurements of the prototype with the input ports terminated with matched loads, and connected in a Van Atta scheme. For the Van Atta case, both passive and amplifier configurations are considered. RCS measurements are provided for the passive case in the principal planes of the antenna. In the amplifier case, only one principal plane is considered. Finally conclusions are drawn in Section VI.

II. Monostatic RCS of a Van Atta array of long slots

Let us consider an array of long slots radiating in free space, as shown in Fig. 1. For simplicity, the slots are fed by air-filled PPW lines. It is assumed that only the principal Transverse Electromagnetic Mode (TEM) is traveling within the feed lines ($w_s < \lambda_u/2$ with λ_u the free space wavelength at the upper extreme of the band of operation). In addition, an ideal Van Atta connection is assumed for the feeding waveguide lines. A practical realization of the Van Atta connection will be presented in Section IV. The monostatic RCS of the finite array of long slots under Van Atta operation can be derived using the approach proposed in [19]. Along the principal planes of the array, the monostatic RCS can be written as:

$$\sigma(\theta) = \frac{\lambda^2}{4\pi} G^2(\theta), \tag{1}$$

where θ, λ and $G(\theta)$ are the elevation angle in the principal planes, the wavelength at the operating frequency and the antenna gain in the considered scanning plane and direction.

In order to derive the gain of the antenna, the radiated field is first calculated. The radiated field of the finite array can be approximated by using a windowing approach. Specifically, the tangential aperture field distribution of the infinite array [20] is used to derive the Fourier Transform (FT) of the tangential field for the finite case. For an array of $N_x \times N_y$ cells, this yields:

$$\tilde{E_x}(k_x, k_y) = \int_{-a_x}^{a_x} \int_{-a_y}^{a_y} E_x(x, y, 0) e^{jk_x x + k_y y} dx dy, \tag{2}$$

where $a_x = (N_x - 1)/2 + d_x/2$, $a_y = (N_y - 1)/2 + d_y/2$, d_x and d_y are the array periods along x and y, and $E_x(x, y, 0)$ is the tangential electric field distribution over the aperture ($z = 0$) for the infinite case (refer to Fig. 1). The period d_x and d_y are chosen smaller than half the wavelength in free space at the highest frequency of operation. A periodicity along the y-axis is also introduced to account for sampling of the aperture along this direction. The tangential electric field in (2) can be expressed as [21]:

$$\begin{aligned} E_x(x, y, 0) &= \frac{V_0}{d_x} \sum_{n=-\infty}^{\infty} \operatorname{sinc}\left(\frac{k_{xn} w_s}{2}\right) e^{-jk_{xn}x} \\ &\quad \sum_{m=-\infty}^{\infty} \operatorname{sinc}\left(\frac{k_{ym} d_y}{2}\right) e^{-jk_{ym}y}, \end{aligned} \tag{3}$$

where $k_{xn} = k_{x0} - 2\pi n/dx$, $k_{ym} = k_{y0} - 2\pi m/dy$, $k_{x0} = k \sin\theta_0 \cos\phi_0$ and $k_{y0} = k \sin\theta_0 \sin\phi_0$ are the transverse Floquet wavenumbers and propagation constants for the array pointing toward (θ_0, ϕ_0), respectively. The variables k and V_0 are the free space propagation constant and amplitude of the considered incident TEM mode, respectively. An expression for V_0 is provided in the Appendix. As opposed to the formulation provided in [21], here we consider only the principal TEM mode and a periodicity along y. Substituting (3) in (2), and after some algebraical manipulations, the FT of the tangential electrical field for the finite case can be written as:

$$\begin{aligned} \tilde{E_x}(k_x, k_y) &= V_0 d_y A F_x A F_y \\ &\quad \sum_{n=-\infty}^{\infty} \operatorname{sinc}\left(\frac{k_{xn} w_s}{2}\right) \operatorname{sinc}\left(\frac{(k_x - k_{xn}) w_s}{2}\right) \\ &\quad \sum_{m=-\infty}^{\infty} \operatorname{sinc}\left(\frac{k_{yn} d_y}{2}\right) \operatorname{sinc}\left(\frac{(k_y - k_{ym}) d_y}{2}\right), \end{aligned} \tag{4}$$

where:

$$AF_x = \sum_{n_x=-(N_x-1)/2}^{(N_x-1)/2} e^{j(k_x-k_{x0})n_x d_x}, \quad (5)$$

$$AF_y = \sum_{m_x=-(N_y-1)/2}^{(N_y-1)/2} e^{j(k_y-k_{y0})n_y d_y}, \quad (6)$$

are the array factors along x and y, respectively.

The far field of the array at the observation point P_0 in Fig. 1 can be then derived using an asymptotic evaluation [22] as:

$$E_\theta(\theta_0,\phi_0) = jk\frac{e^{-jkr}}{2\pi r}\cos(\phi_0)\frac{1+\cos(\theta_0)}{2}\tilde{E_x}, \quad (7)$$

$$E_\phi(\theta_0,\phi_0) = -jk\frac{e^{-jkr}}{2\pi r}\cos(\phi_0)\frac{1+\cos(\theta_0)}{2}\tilde{E_x}, \quad (8)$$

For a Van Atta operation $k_x = k_{x0}$ and $k_y = k_{y0}$, therefore (4) simplifies in:

$$\tilde{E_x}(k_{x0},k_{y0}) = V_0 d_y N_x N_y \,\mathrm{sinc}\left(\frac{k_{x0}w_s}{2}\right)\mathrm{sinc}\left(\frac{k_{y0}d_y}{2}\right) \quad (9)$$

Along the principal scanning planes, the gain of the antenna under a Van Atta operation is then expressed as:

$$G(\theta_0,\phi_0=0^\circ,90^\circ) = \frac{4\pi|rE_{\theta/\phi}|^2}{2\eta N_x N_y P_{in}}, \quad (10)$$

with P_{in} the input power at a generic PPW line and η the free space impedance. By noticing that the expressions for E_θ and E_ϕ differ only for a sign, we can write the gain of the array along the principal planes in a compact form as:

$$G(\theta_0) = \frac{\pi}{\lambda^2}|1+\cos\theta_0|^2(1-|S_{act}|^2)N_x N_y d_x d_y \,\mathrm{sinc}^2\left(\frac{k_{x0}w_s}{2}\right)\mathrm{sinc}^2\left(\frac{k_{y0}d_y}{2}\right), \quad (11)$$

where S_{act} denotes the active reflection coefficient of the array, as given in the Appendix. The quantity $N_x N_y d_x d_y$ in (11) corresponds to the geometrical area A of the finite array. Finally, (11) is used in (1) to derive the monostatic RCS along the principal scanning planes of the array:

$$\sigma(\theta_0) = \frac{\pi}{4\lambda^2}|1+\cos\theta_0|^4(1-|S_{act}|^2)^2A^2, \,\mathrm{sinc}^4\left(\frac{k_{x0}w_s}{2}\right)\mathrm{sinc}^4\left(\frac{k_{y0}d_y}{2}\right), \quad (12)$$

In order to gain some insight into the operation of the antenna as Van Atta reflector, let us consider the case where $d_x \approx w_s$ and the antenna operates at a low frequency: its periods d_x and d_y are very small with respect to the wavelength (an over-sampled aperture). In this case, the active reflection coefficient of the array along both planes (refer to the Appendix) is:

$$S_{act} = \frac{1-\cos\theta_0}{1+\cos\theta_0}, \quad (13)$$

and the $\mathrm{sinc}(.)$ terms in (12) are approximated to 1. The monostatic RCS then reduces to:

$$\sigma(\theta) = \frac{4\pi}{\lambda^2}A^2\cos^2\theta. \quad (14)$$

This expression corresponds to the ideal monostatic RCS of an antenna with area A [18]. Therefore, arrays of long slots with very small periodicities with respect to the wavelength are the best antenna solution for Van Atta arrays, and are superior to any solution based on resonant elements such as patches or dipoles. Furthermore (14) confirms that the proposed array can collect and retransmit all the power impinging on its aperture, as also proven in [14] and shown later in Section III

III. Array of long slots: design

The unit cell of the proposed array of long slots is shown in Fig. 2. The design frequency of the array is $f_0 = 5.8$ GHz. The slot width w_s and periodicity d_y along y are equal to $0.45\lambda_0 = 23$ mm and $0.46\lambda_0 = 24$ mm (λ_0 is the wavelength in free space at f_0), respectively. They have been chosen following the guidelines provided in [21], [23]. The design goals were an input reflection coefficient lower than -10 dB in the band $5.4-6.2$ GHz, for a scanning range of $\pm 30^\circ$ in both the E- (xz-plane in Fig. 2a) and H-planes (yz-plane in Fig. 2a). This scanning range is suitable for a WPT system operating in a room within a public environment [3]. However more extreme cases could be covered by the proposed array [23].

The long slots are fed by air-filled PPW lines (refer to Fig. 1). Each PPW of the unit cell is terminated with a coaxial input port with a 50 Ohm impedance. The input ports are separated by a distance $d_x = 0.46\lambda_0 = 24$ mm in the array. The matching network is shown in Fig. 2b. Specifically, the active impedance of the slots is matched to the input PPW line using a two stage transformer. The input ports are then matched to the PPW lines by a coaxial probe transition [24].

Plotted in Fig. 3 is the active reflection and transmission coefficients of the unit cell. The results have been obtained using Ansys HFSS. The unit cell in Fig. 2 has been simulated within an infinite array environment, with the air box above the structure terminated in a Floquet port. The active reflection coefficient refers to the input reflection coefficient at the coaxial input port (SMA connection in Fig. 2). The active transmission coefficient refers to the power transferred from the coaxial input port to the Floquet port, for a field polarized along the x-axis. The antenna is matched over a scanning range of $\pm 40^\circ$ in both principal planes, within a 24% fractional bandwidth. In addition, the active transmission coefficient shows that the antenna can absorb and retransmit the full power impinging from a remote source as outlined in [14]. This is a major advance with respect to arrays of resonant elements [3], [14]. Note that similar performance, in transmission and reception, can be achieved with wide angle, wideband scanning antennas such as connected arrays [25].

IV. Prototype

A. Array

The finite array is made up by four slots, each fed by eight coaxial probes through SMA connectors, resulting in 32 ports. The final prototype has been fabricated using a CNC milling process. The antenna is composed of several simpler blocks made of aluminum. The various blocks are assembled using dowels and screws in a manner similar to

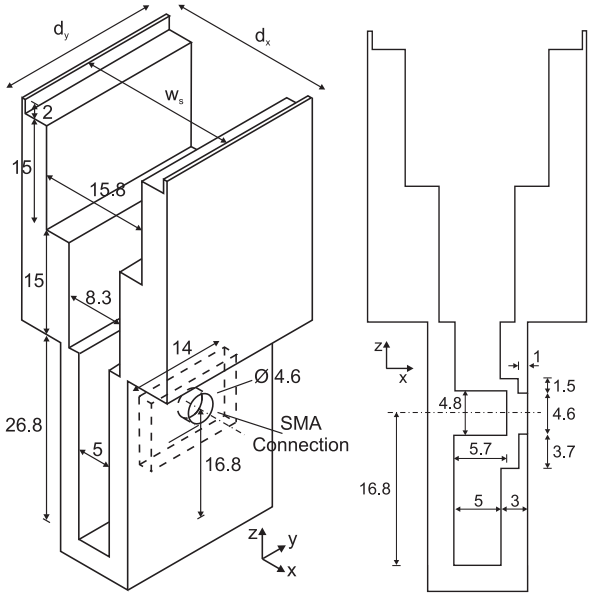

(a) (b)

Fig. 2. A unit cell of the array of long slots. (a) Prospective view. (b) Cut-view along the xz-plane. The dimensions are in mm. The period, $d_x = d_y$, and the slot width, w_s, are equal to 24 mm and 23 mm, respectively.

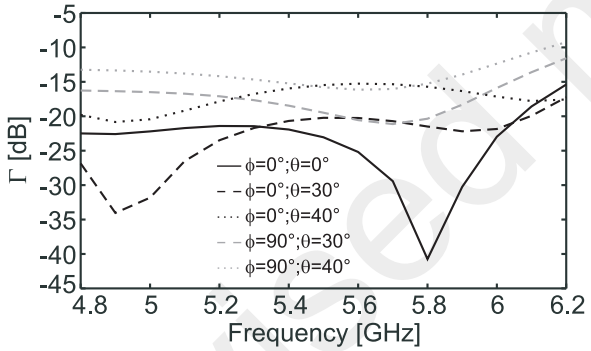

(a)

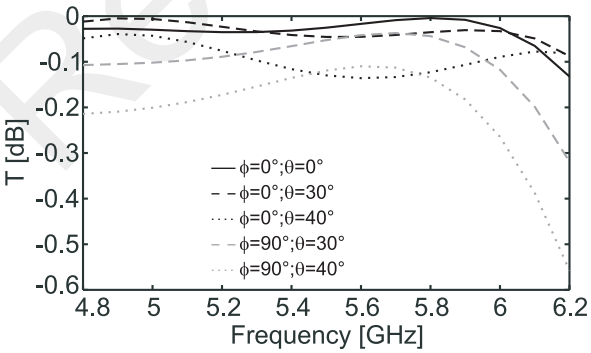

(b)

Fig. 3. Active reflection (a), and transmission (b) coefficients for the unit cell in an infinite periodic environment.

that presented in [23]. An accuracy better than 50μm was achieved in fabrication and alignment. Bonding processes or electromagnetic chokes were not required, reducing the complexity and cost of the overall structure. The completed prototype is shown in Fig. 4. The SMA connectors of the input ports can be seen. Coaxial cables of length 30.48 cm were used to access the input ports of the array. Female-to-female adapters were used to pair the input ports into a Van Atta scheme (as shown in Fig. 4) through the coaxial cables.

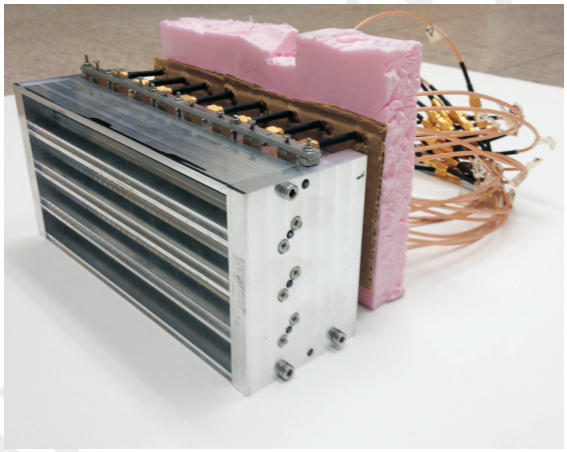

Fig. 4. Prototype of the finite array of long slots. The input ports are connected in a Van Atta scheme. The coaxial cables used to connect the input ports and the female-to-female adapters are shown.

B. Bi-direction amplifier

The configuration of the bi-directional amplifier employed in the measurements is shown in Fig. 5 [26], [27]. The amplification is achieved using unilateral amplifiers on two electrical paths separated by circulators. The final setup is shown in Fig. 6. Off-the-shelf components were used for the various elements in Fig. 5. The amplifiers are ZX60-8000E-S+ components from Mini-Circuits with a nominal gain of 8.36 dB at 5.8 GHz [28]. The circulators are made by cascading a dual (FMCR1019, insertion loss < 0.2 dB, isolation < -50 dB [29]) and a single (SFC4080B [30] insertion loss < 0.3 dB, isolation < -20 dB) junction circulator from Fairview Microwave. This configuration allows for good isolation between the two branches of the bi-directional amplifier. The unused ports of the circulators are terminated with 50 Ohm loads. The various components are connected using coaxial cables of length 15.24 mm. This bi-directional amplifier was preferred over more advanced configurations [31], [32], due to its simple implementation. In addition, the same radiating element and polarization can be used in reception and re-transmission [32].

The scattering matrices for two versions of the proposed amplifier have been measured, with the unilateral amplifiers fed with a 12 V DC voltage source. The matching and transmission coefficients are provided in Figs. 7a and b for the two bi-directional amplifiers used in Section V. Fairly good impedance matching is observed in the band 4.8-6.8 GHz with an amplification in both directions of about 5 dB. The phase

difference between the input and output ports of the amplifiers is shown in Fig. 7c. A phase error smaller than 30° (smaller than a tenth of the free space wavelength) is observed for one of the two amplifiers in the considered band. The performances of the amplifiers are thus considered acceptable within the possible tolerances of their building blocks. For comparison, the scattering parameters of the unbiased case (voltage source turned off) are also shown. The unbiased configuration is matched, with transmission coefficients lower than -20 dB (across the band) with respect to the biased case.

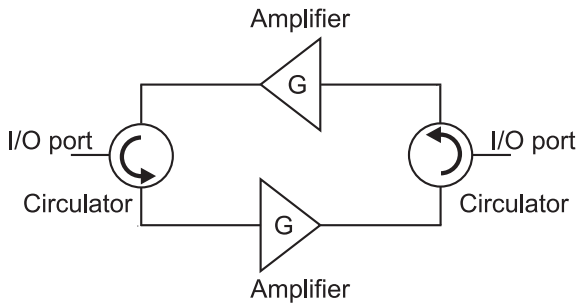

Fig. 5. Circuit schematic of the adopted bi-directional amplifier.

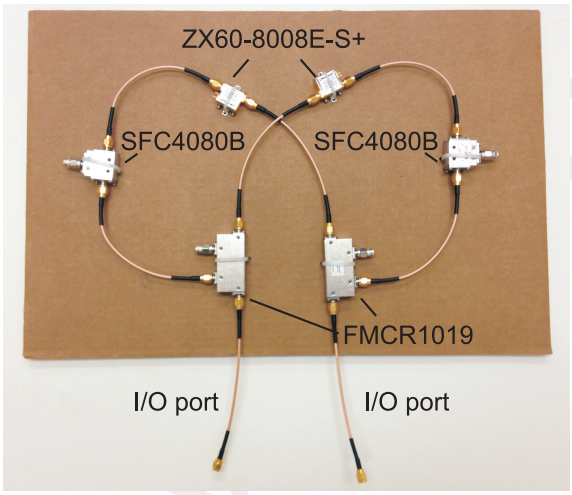

Fig. 6. Implementation of the bi-directional amplifier using off-the-shelf components.

V. Measurements

In the following section, the measured monostatic RCS is provided for two cases: passive (without bi-directional amplifiers), and active (with bi-directional amplifiers). The measurements have been performed in the anechoic chamber at the University of Michigan using a radar setup consisting of a vector network analyzer and two standard gain horns [19]. The two horns were placed side by side at distance of about 14 m from the antenna located on a rotating arm. The angular offset of the horn with respect to the antenna was smaller than 1°. The reflected signal from the antenna was measured over the azimuthal and elevation planes by physically rotating both the antenna and the horns by 90°. The measurements were

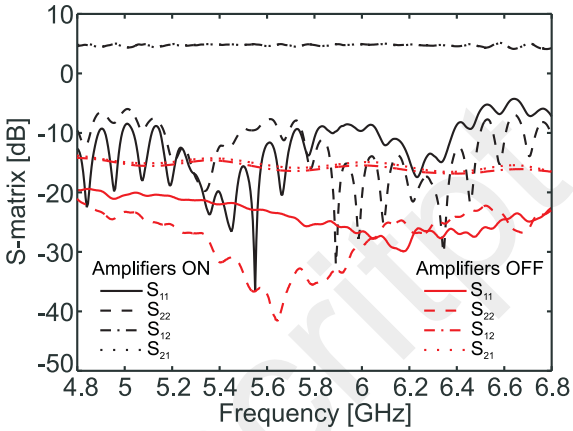

(a)

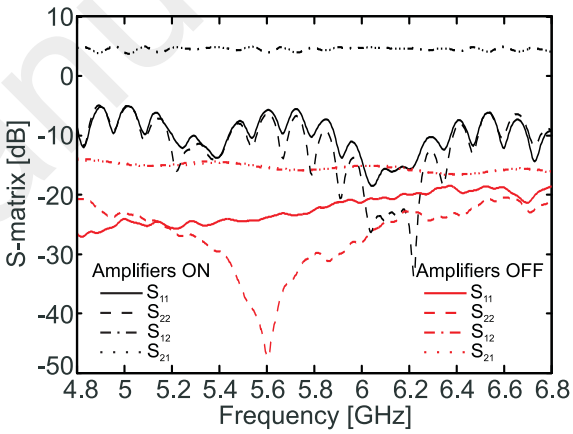

(b)

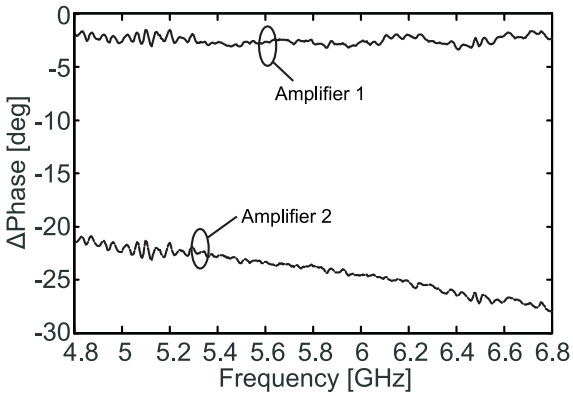

(c)

Fig. 7. Measured scattering parameters of two bi-directional amplifiers shown in Fig. 6. Scattering parameters of the biased and unbiased case (a) Amplifier 1; (b) Amplifier 2 (b); (c) Phase difference between the transmission coefficients ($arg(S_{21}) - arg(S_{12})$).

performed over the band $4.8 - 6.8$ GHz across an angular range of $\pm 90°$, with a step of $1°$. The response from the antenna was time gated to reduce the interferences of the measurement setup (coupling between the horns, reflection from cables, antenna support, etc). For the passive case, the RCS is provided in both the principal planes of the radiating structure. On the other hand, only the monostatic RCS over the E-plane (xz-plane in Fig.2) has been measured for the active case to reduce the complexity of the feeding system, as described in Section V-B.

A. Passive case

The normalized monostatic RCS of the passive array, with the input ports connected in a Van Atta arrangement, is given in Fig 8 along both principal planes at 5.8 GHz. The -3 dB (-10 dB) beamwidth is approximately $54°$ ($118°$) and $50°$ ($80°$) in the E- and H-plane, respectively. The results demonstrate the large field of view of the proposed array. The measured normalized monostatic RCS of the antenna with a metallic plate (96×214 mm^2) covering its aperture is shown for comparison. The monostatic RCS computed using Ansys HFSS is also reported. In this case, the finite array has been simulated and the monostatic RCS calculated using (1). Note that the simulated array did not include the cables and adaptors used in the final prototype. However, in both planes we have good agreement between the measured and simulated RCS, showing that the proposed antenna has enhanced tracking capabilities. In other words, the antenna would be able to track and transfer power to any electronic device in need of energy over a large field of view.

The monostatic RCS of the antenna, with the input ports terminated in 50 Ohm loads is also shown for both planes. The RCS is reduced by more than 12 dB with respect to the Van Atta case. Along the E-plane, we notice a slight asymmetry in the RCS due to the metallic support used for the SMA connectors that is visible in Fig. 4. This result confirms that the antenna does not scatter energy when the input ports are matched. This is in stark contrast to arrays of resonant elements [3], [11]-[18].

The wide band behaviour of the proposed array is evident from the RCS performance of the antenna. Figs. 9(a) and (b) provides the measured, normalized monostatic RCS of the array in the H- and E-planes, respectively. The conclusion reached for the central frequency can be extended to the entire band ($4.8 - 6.2$ GHz). Such a wideband operation is not possible with retrodirective arrays made of resonant elements [9], [26]. The operation of the proposed array over a large field of view and bandwidth can be useful for pulsed power transmission.

B. Active case

The operation of the proposed array in the active mode requires 16 bi-directional amplifiers to be connected to pairs of input ports [11]. To reduce the complexity and cost of the measurement setup, the active configuration has been tested only for operation along the E-plane. In this case, the eight input ports feeding each slot were connected to four uniform

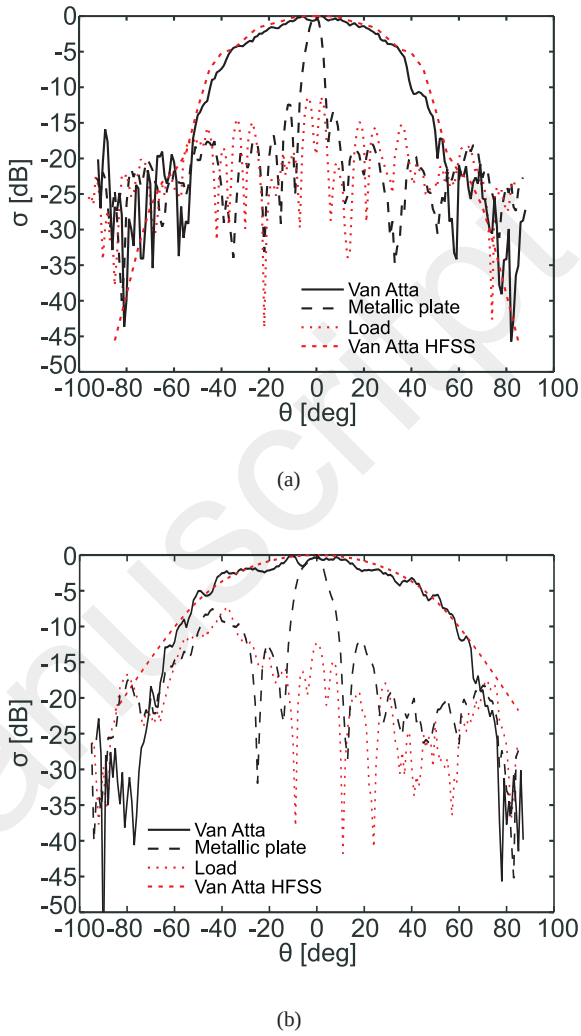

Fig. 8. Measured monostatic RCS of the array along the principal planes. (a) H-plane (yz-plane in Fig. 2); (b) E-plane (xz-plane in Fig. 2). The monostatic RCS of the array with the radiating aperture covered by a metallic plate of the same cross section is also plotted.

power dividers in microstrip technology using 30.48 cm long coaxial cables. This arrangement reduces the number of input ports to be connected in a Van Atta configuration to four. Therefore, only two of the bi-directional amplifiers presented in Section IV are required. The experimental setup is shown in Fig. 10, which depicts the various elements (antenna, power dividers, bi-directional amplifiers). Note that flexible cables have been used to connect the antenna to the power dividers and amplifiers. However, more integrated solutions can be envisaged in the future for compactness.

The uniform power dividers were fabricated by laser etching a double grounded substrate Rogers TM/Duroid 5880 with permittivity 2.2 and thickness 1.575 mm. The input and output ports of the power dividers are 50 Ohm, and connected to SMA connectors. Fig.11 shows the input reflection coefficient for the power dividers with the eight output ports terminated in 50 Ohm loads. The measurements are in agreement with simulation results, and show a reflection coefficient lower than

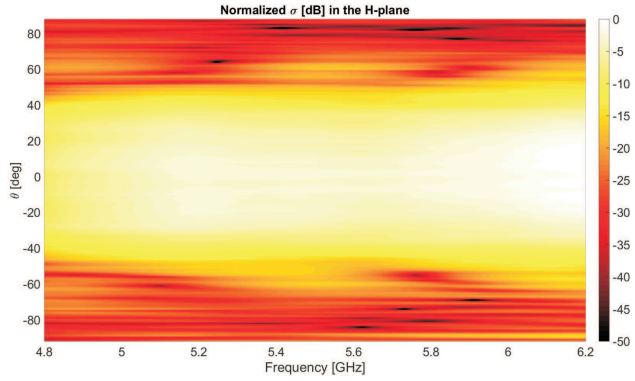

(a)

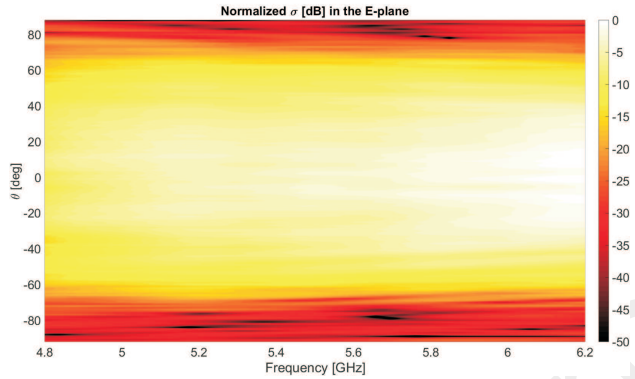

(b)

Fig. 9. Measured monostatic RCS of the array along the principal planes over the $4.8-6.2$ GHz frequency band . (a) H-plane (yz-plane in Fig. 2); (b) E-plane (xz-plane in Fig. 2).

-10 dB in the $4.8-6.4$ GHz band. Note that the four power dividers do not present exactly the same matching response due to fabrication tolerances and misalignments in the soldered SMA connectors.

The monostatic RCS of the active array along the E-plane is shown in Fig. 12a, at 5.8 GHz. The -3 dB (-10 dB) beamwidth is approximately $70°$ ($106°$), showing the large field of view of the proposed structure. The normalized monostatic RCS of the simulated passive structure, as in Fig. 8, is provided for comparison. Fairly good agreement is observed between measurement and simulation. In particular, the measurement results show ripples of about 1dB in the main lobe. This is attributed to the spurious reflections at the input ports of the bidirectional amplifiers evident in the scattering parameters of Fig. 7. These reflections are also responsible for the reduced field of view with respect to the passive case in Fig. 8. Nevertheless, the performance is stable within the considered frequency range, as shown in Fig. 12b.

The RCS of the unbiased case is also provided for comparison. The RCS is reduced by approximately 10 dB with respect to the biased case. The results clear show that the proposed antenna can be used in a WPT scenario to detect

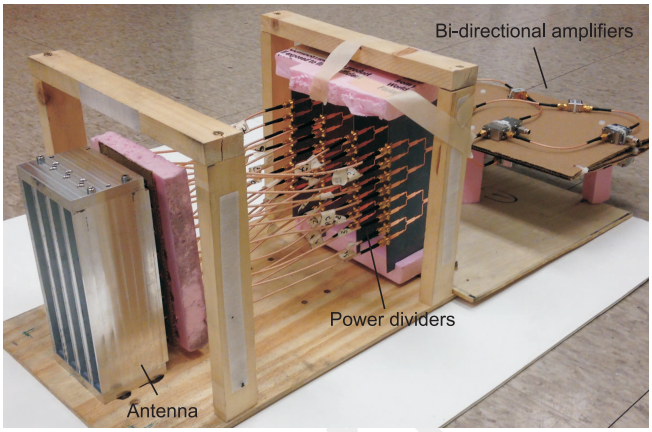

Fig. 10. Prototype of the finite array of long slots connected to two bi-directional amplifiers for scanning along the E-plane. The input ports of the array are connected to the amplifiers through four uniform power dividers made in microstrip technology.

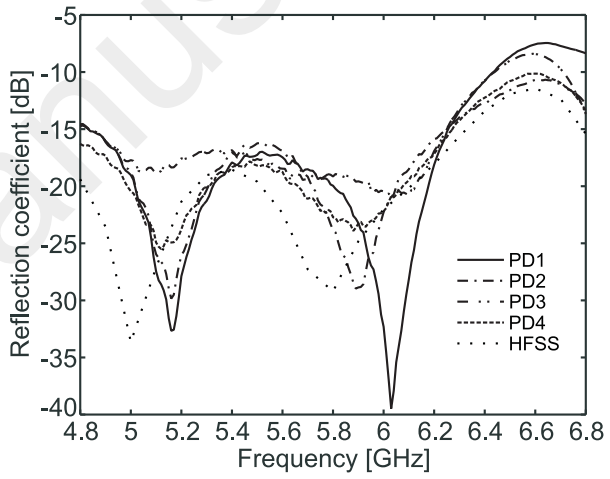

Fig. 11. Reflection coefficient of the four uniform power dividers used to connect the input ports of the array to the bi-directional amplifiers, as shown in Fig 10. PD stands for power divider.

and re-transmit power to a mobile user over a large field of view and bandwidth.

VI. Conclusion

The monostatic RCS of a Van Atta array of long slots has been derived. It has been shown that such an antenna behaves as an ideal Van Atta reflector, over a large band and field of view, for periodicities much smaller than the wavelength. The proposed antenna is optimal for WPT applications and for applications requiring fast tracking of a moving user. The design and measurement results of the Van Atta array of long slots has then been presented. The designed array consists of four slots, each fed by eight SMA connectors. Therefore, the array has 32 input ports. Coaxial cables are used to connect pairs of input ports in a Van Atta arrangement. The prototype array is made from aluminium using a standard CNC milling process. Monostatic RCS measurements show a -3 dB (-10 dB) beamwidth of approximately $54°$ ($118°$) and $50°$ ($80°$) in the E- and H-plane, respectively, over a

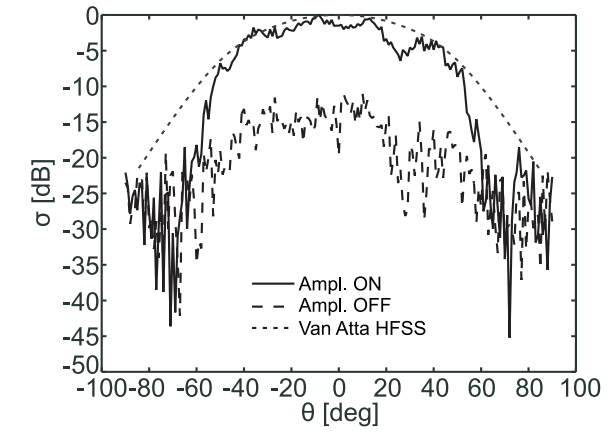

(a)

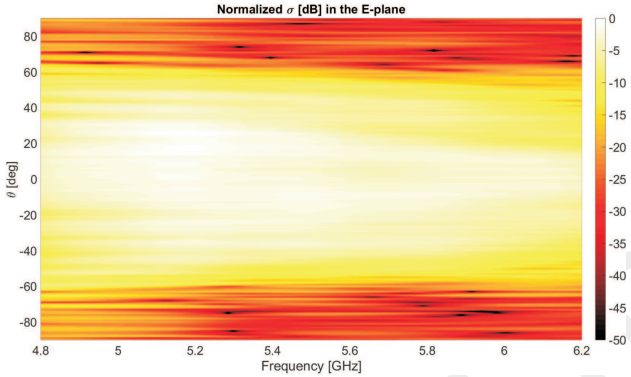

(b)

Fig. 12. Measured monostatic RCS of the array along the E-plane for the active case. (a) Operating frequency of 5.8 GHz. The results when the unilateral amplifiers are unbiased is also plotted for comparison. (b) RCS vs. frequency over $4.8-6.2$ GHz band.

$4.8-6.2$ GHz band. In addition, it is shown that the antenna does not backscatter impinging radiation when terminated with matched loads. This is in contrast to classical designs based on resonant elements. The results clearly confirm that the proposed antenna can track moving users with reduced backscattering and enhanced efficiency over a large field of view and wide bandwidth.

An active configuration is also tested along the E-plane of the proposed array. In particular, four uniform power dividers are used to connected the input ports of the array to two bi-directional amplifiers. The bi-directional amplifiers are made from off-the-shelf components. The active array also exhibits a large field of view and a gain of more than 10 dB with respect to the unbiased case. The proposed solution may pave the way toward active transponders for wireless power transmission with a large field of view. In addition, the wide operation band of the design can be useful for pulsed power transmission.

APPENDIX

The term V_0 in (3) can be obtained by equating the radiated power to the input power feeding the antenna through the PPW lines, yielding:

$$V_0 = \sqrt{\frac{2P_{in}(1-|S_{act}|^2)}{dy/\eta d_x}}, \tag{15}$$

where P_{in}, S_{act} and η are the input power over the array, the active reflection coefficient for scanning at (θ_0, ϕ_0), and η is the free space impedance. The active reflection coefficient can be derived from the active admittance of the array as [21]:

$$S_{act} = \frac{-Y_{act} + w_s/\eta d_y}{Y_{act} + w_s/\eta d_y}, \tag{16}$$

with Y_{act} given by:

$$Y_{act} = \frac{d_y}{\eta d_x} \sum_{n=-\infty}^{n=\infty} \sum_{m=-\infty}^{m=\infty} \mathrm{sinc}^2\left(\frac{k_{xn} w_s}{2}\right) \mathrm{sinc}^2\left(\frac{k_{ym} d_y}{2}\right) \frac{k^2 - k_{ym}^2}{k k_z}, \tag{17}$$

where $k_{xn} = k_{x0} - 2\pi n/d_x$, $k_{ym} = k_{y0} - 2\pi m/d_y$ and $k_z = \sqrt{k^2 - k_{xn}^2 - k_{ym}^2}$.

REFERENCES

[1] K. Wu, D. Choudhury, and H. Matsumoto, "Wireless power transmission, technology, and applications," *Proc. IEEE*, Vol. 101, No. 6, pp. 1271 - 1275, June 2013.

[2] S. Y. R. Hui, W. Zhong, and C. K. Lee, "A critical review of the recent progress in mid-range wireless power transfer," *IEEE Trans. Power Electron.*, Vol. 29, No. 9, pp. 4500 4511, Sept. 2014.

[3] Y. Li and V. Jandhyala, "Design of retrodirective antenna arrays for short-range wireless power transmission," *IEEE Trans. Antennas Propag.*, Vol. 60, No. 1, pp. 206 - 211, July 2012.

[4] X. Wang, S. Sha, J. He, L. Guo, and M. Lu, "Wireless power delivery to low-power mobile devices based on retro-reflective beamforming," *IEEE Antennas Wireless Propag. Lett.*, Vol. 13, pp. 919 - 922, 2014.

[5] H. Zeine, "Wireless power transmission system," U.S. Patent 8,159,364, Apr. 17, 2012.

[6] E. J. Putzer and R. N. Ghose, "Redirective and retrodirective antenna arrays," *IEEE Trans. Antennas Propag.*, Vol. 17, No. 3, pp. 276 - 279, May 1969.

[7] J. de Rosny, G. Lerosey, and M. Fink, "Theory of electromagentic time-reversal mirrors," *IEEE Trans. Antennas Propag.*, Vol. 58, No. 10, pp. 3139 - 3149, Oct. 2010.

[8] V. Fusco and N. Buchanan, "Developments in retrodirective array technology," *IET Microw. Antennas Propagat.*, Vol. 7, No. 2, pp. 131 - 140, 2013.

[9] K. M. K. H. Leong, R. Y. Miyamoto, and T. Itoh, "Moving forward in retrodirective antenna arrays," *IEEE Potentials*, Vol. 22, No. 3, pp. 16 - 21, Aug.-Sept. 2003.

[10] N. Shinohara, "Beam control technologies with a high-efficiency phased array for microwave power transmission in Japan," *IEEE Proc. IEEE*, Vol. 101, No. 6, pp. 1448 1463, June 2013.

[11] L. C. Van Atta, "Electromagnetic reflector," U.S. Patent 2,908,002, Oct. 6, 1959.

[12] G. S. Shiroma, R. Y. Miyamot, and W. A. Shiroma, "A 16-element two-dimensional active self-steering array using self-oscillating mixers," *IEEE Trans. Microw. Theory Techn.*, Vol. 51, No. 12, pp. 2476 - 2482, Dec. 2003.

[13] C. Y. Pon, "Retrodirective array using the heterodyne technique," *IEEE Trans. Antennas Propag.*, Vol. 12, No. 2, pp. 176 - 180, Mar. 1964.

[14] M. Ettorre, W. A. Alomar, and A. Grbic, "Radiative wireless power transfer system using wideband, wideangle slot arrays," under review in *IEEE Trans. Antennas Propag.*, Aug. 2016.

[15] E. D. Sharp and M. A. Diab, "Van Atta reflector array," *IRE Trans. Antennas Propag.*, Vol. 8, No. 4, pp. 436 - 438, July 1960.

[16] J. Appel-Hansen, “A Van Atta array consisting of hal-wave dipoles,” *IEEE Trans. Antennas Propag.*, Vol. 14, No. 6, pp. 694 - 700, Nov. 1966.
[17] E. D. Nielsen, “Square Van Atta reflector with conducting mounting plane,” *IEEE Trans. Antennas Propag.*, Vol. 18, No. 1, pp. 48 - 54, Jan. 1970.
[18] B. L. Lewis, “Efficient wide-angle coverage dipole Van Atta array design,” *IEEE Trans. Antennas Propag.*, Vol. 16, No. 2, p. 256, Mar. 1968.
[19] S. Christie, R. Cahill, N. B. Buchanan, V. Fusco, N. Mitchell, Y. V. Munro, and G. Maxwell-Cox, “Rotman lens-based retrodirective array,” *IEEE Trans. Antennas Propag.*, Vol. 60, No. 3, pp. 1343 - 1351, Mar. 2012.
[20] A. Ishimaru, R. J. Coe, G. E. Miller, and W. P. Geren, “Finite periodic structure approach to large scanning array problems,” *IEEE Trans. Antennas Propag.*, Vol. AP-33, No. 11, pp. 1213 - 1220, Nov. 1985.
[21] F. Foglia Manzillo, M. Ettorre, M. Casaletti, N. Capet, and R. Sauleau, “Active impedance of infinite parallel-fed continuous transverse stub arrays,” *IEEE Trans. Antennas Propag.*, Vol. 63, No. 7, pp. 3291 - 3297, July 2015.
[22] C. A. Balanis, *Antenna Theory: Analysis and Design*, 2nd ed., John Wiley & Sons, Inc., New York, 1997.
[23] M. Ettorre, F. Foglia Manzillo, M. Casaletti, R. Sauleau, L. Le Coq, and N. Capet, “Continuous transverse stub array for Ka-band applications,” *IEEE Trans. Antennas Propag.*, vol. 63, No. 11, pp. 4792 - 4800, Nov. 2015.
[24] D. M. Pozar, *Microwave engineering*, 4nd ed., John Wiley & Sons, Inc., New York, 2012.
[25] D. Cavallo, A. Neto, and G. Gerini, “Green’s function based equivalent circuits for connected arrays in transmission and in reception,” *IEEE Trans. Antennas Propag.*, Vol. 59, No. 5, pp. 1535 - 1545, May 2011.
[26] V. F. Fusco and S. L. Karode, “Self-phasing antenna array techniques for mobile communications applications,” *Electron. Comms. Eng. J.*, Vol. 11, No. 6, pp. 279 - 286, Dec. 1999.
[27] C. C. Cutler, R. Kompfner, and L. C. Tillotson, “A self steering array repeater,” *Bell Syst. Tech. J.* , Vol. 42, No. 5, pp. 2013 - 2032, Sept. 1963.
[28] Datasheet Amplifiers ZX60-8008E-S+ from Mini-Circuit [Online]. Available: https://www.minicircuits.com/pdfs/ZX60-8008E+.pdf
[29] Datasheet FMCR1019 circulator from Fairview Microwave [Online]. Available: https://www.fairviewmicrowave.com/images/productPDF/FMCR1019.pdf
[30] Datasheet SFC4080B circulator from Fairview Microwave [Online]. Available: https://www.fairviewmicrowave.com/images/productPDF/SFC4080B.pdf
[31] H.-T. Chen and S.-J. Chung, “Design of a planar array transponder with broad responding beam,” *IEEE Microw. Guided Wave Lett.*, Vol. 7, No. 9, pp. 297 - 299, Sept. 1997.
[32] S.-J. Chung, S.-M. Chen, and Y.-C. Lee, “A novel bi-directional amplifier with applications in active Van Atta retrodirective arrays,” *IEEE Trans. Antennas Propag.*, Vol. 51, No. 2, pp. 542 - 547, Feb. 2003.